

Implicit Hypothesis Testing and Divergence Preservation in Neural Network Representations

Kadircan Aksoy^{1,2} Peter Jung^{1,2} Protim Bhattacharjee²

Abstract

We study the supervised training dynamics of neural classifiers through the lens of binary hypothesis testing. We model classification as a set of binary tests between class-conditional distributions of representations and empirically show that, along training trajectories, well-generalizing networks increasingly align with Neyman–Pearson optimal decision rules via monotonic improvements in KL divergence that relate to error rate exponents. We finally discuss how this yields an explanation and possible training or regularization strategies for different classes of neural networks.

1. Introduction

Supervised classification can be viewed fundamentally as a statistical hypothesis testing problem: given input samples $x \sim \mathcal{X}$ and associated labels $y \sim \mathcal{Y}$ such that there is a non-trivial conditional relation between the two, the task of a classifier is to decide, for each observation x , between competing hypotheses corresponding to class-conditional distributions $\{\mathbb{P}(X|Y = y) \mid \forall y \in \mathcal{Y}\}$.

Classical decision theory characterizes the optimal solution to this, in the binary case, via likelihood ratio tests and the Neyman–Pearson (NP) lemma, which establishes optimal trade-offs between type-I and type-II errors in terms of likelihood ratios and Kullback–Leibler (KL) divergence (Kullback & Leibler, 1951). Despite the widespread success of deep neural networks as classifiers, the relationship between modern training dynamics and this classical hypothesis testing framework remains poorly understood. In particular, it is unclear whether backpropagation implicitly steers learned representations toward statistically optimal decision regions.

Our contributions in closing this gap are as follows:

¹Communications and Information Theory, Technical University Berlin, Berlin, Germany ²Institute for Space Research, German Aerospace Center, Berlin, Germany. Correspondence to: Kadircan Aksoy <kadircan.aksoy@dlr.de>.

- Formalize supervised classification as a sequence of binary hypothesis tests on learned representations, making explicit the connection between neural networks and classical hypothesis testing theory.
- Introduce a controlled synthetic classification setting with analytically known class-conditional KL divergences, enabling comparison between learned decision rules and statistically optimal tests.
- Show how training dynamics of classifier networks can be interpreted in terms of induced likelihood ratio tests between class-conditional feature distributions.
- Conclude empirically that adequately trained neural classifiers produce outputs that serve as sufficient statistics for the log-likelihood ratio (LLR) test, thereby achieving Neyman–Pearson optimal performance.

2. Related Work

The gap between the complexity of modern neural networks and principled tools for analyzing and interpreting their behavior has been an important topic of recent discussion (Zhang et al., 2021). The Information Bottleneck (IB) was proposed as a global theory of learning dynamics, framing training as a trade-off between predictive information $I(T; Y)$ and representational complexity $I(X; T)$ (Shwartz-Ziv & Tishby, 2017) with T denoting the network output. However, IB has been criticized on two main grounds: (i) for deterministic networks, $I(X; T)$ is typically ill-posed (constant or infinite); and (ii) mutual information measurements rely on high-dimensional histogram density estimates, which are known to be unreliable (Saxe et al., 2019). (Kolchinsky et al., 2018). These issues have motivated extensions that replace or refine the tracked quantities, including generalized-IB and other partial information decompositions (Westphal et al., 2025) (Tax et al., 2017).

In contrast, explainable AI (xAI) methods focus on local interpretability, producing per-sample explanations via sensitivity analysis, local surrogate models, or feature attributions (see e.g. (Montavon et al., 2019), (Ribeiro et al., 2016)). While diagnostically useful, such methods do not define a distribution-level object and lack a ground-truth notion of correctness (Rawal et al., 2025).

Information-theoretic quantities therefore remain attractive for global analysis: they are invariant under invertible reparameterizations and admit operational interpretations in coding, prediction, and statistical decision-making. Their usefulness, however, depends critically on whether the quantities are well-defined for modern architectures and can be estimated reliably—precisely the issues that motivate alternative formulations and estimators beyond classical IB (Saxe et al., 2019).

(Anders & Korn, 1999) proposes a model selection procedure for neural networks based on hypothesis testing, (as opposed to, for example, cross validation) by iteratively expanding network topology and performing hypothesis tests on whether the added units correlate with residuals of the original network. Similarly (Mandel & Barnett, 2024) suggests a hypothesis testing framework for input feature attribution, akin to local xAI methods. However, to the best of our knowledge, directly interpreting a neural network as a hypothesis test is not an approach pursued before.

3. Theoretical Background

In this section we describe the theoretical framework of binary hypothesis testing and its application to neural networks in detail.

3.1. Binary Hypothesis Testing

Let Z be any random variable, distributed according to a probability distribution $P_0 = \mathbb{P}(H_0)$ or $P_1 = \mathbb{P}(H_1)$, which is not known a-priori. The goal of hypothesis testing is to determine which is the true distribution of Z . It is typically assumed that $Z \sim P_0$ and a test is an algorithm for accepting $Z \sim P_1$ instead, under certain conditions. The Neyman-Pearson Lemma states (Neyman & Pearson, 1933):

Given a fixed rate of false positive errors (FPR), $\alpha := \mathbb{E}_{P_0}[\text{Accept } H_1]$, the log-likelihood-ratio (LLR) test is uniformly most powerful, in the sense that it has the lowest false negative (FNR) error rate, $\beta := \mathbb{E}_{P_1}[\text{Accept } H_0]$:

$$\text{Accept } H_1 \text{ if } \Lambda(z) = \ln \frac{p_1(z)}{p_0(z)} \geq \gamma \quad (1)$$

for any $z \sim Z$, where $\gamma \in \mathbb{R}$ is a constant. Intuitively, $\Lambda(z)$ quantifies the amount of evidence in favor of H_1 over H_0 given by the sample z . If it is positive, this means z is more likely to occur under H_1 .

Stein's Lemma (Chernoff, 1956) gives a bound on the asymptotic case when many samples are available. Suppose n i.i.d samples are drawn from Z ; let $z^n = (z_1, z_2, \dots, z_n)$, $z_i \sim Z$ and P_0^n, P_1^n denote the n -fold product distributions, such that $p_0^n(z^n) = \prod_{i=1}^n p_0(z_i)$ and $p_1^n(z^n) = \prod_{i=1}^n p_1(z_i)$.

Fix the false positive error rate again as $\alpha_n := \mathbb{P}_{P_0^n}[\text{Accept } H_1] \leq \epsilon$ for some $\epsilon \geq 0$. Then the best achievable false negative error is:

$$\beta_n^* := \min_{\text{Test: } \alpha_n \leq \epsilon} \mathbb{P}_{P_1^n}[\text{Accept } H_0] \quad (2)$$

and it satisfies

$$\lim_{\epsilon \rightarrow 0} \lim_{n \rightarrow \infty} -\frac{1}{n} \log \beta_n^* = D_{KL}(P_1 \| P_0) = \mathbb{E}_{P_1} \left[\log \frac{dP_1}{dP_0} \right] \quad (3)$$

where D_{KL} is the KL divergence between P_1 and P_0 .

3.2. Stein's Lemma for Neural Networks

We now relate this to the empirical performance of neural classifiers. Let $X_c := \mathbb{P}(X|Y = c)$, $X_{\bar{c}} := \mathbb{P}(X|Y \neq c)$ be the class conditioned input distributions, where $X_{\bar{c}}$ denotes the mixture of all classes except c ; $X_y, y \neq c$. Suppose we have a K class, balanced classification problem such that $\mathbb{P}(Y = c) = \frac{1}{K}, \forall c \in \mathcal{Y}$. We now define the following joint probability distributions:

$$P(X = x, Y = c) = \frac{1}{K} X_c(x) \quad (4)$$

$$Q(X = x, Y = c) = \frac{1}{K} X_{\bar{c}}(x) \quad (5)$$

which define the hypothesis test

$$H_0 : (X, Y) \sim P \text{ vs. } H_1 : (X, Y) \sim Q. \quad (6)$$

Intuitively, this test asks, given an input sample and class pair (x, c) , is the sample x of class c , or of any other class. Then by the Neyman-Pearson Lemma, the optimal test, given a fixed type-1 error rate α is the following:

$$\Lambda(x, c) = \frac{p(x, c)}{q(x, c)} = \frac{X_c(x)}{X_{\bar{c}}(x)} \geq \mu \quad (7)$$

for some constant μ . However, implementing this test requires knowledge of the conditional distributions $\mathbb{P}(X|Y = c)$ and $\mathbb{P}(X|Y \neq c)$. In high-dimensional settings, plug-in estimation of these densities is statistically inefficient and unstable (Wang & Scott, 2019). We argue that a neural network implementing a (possibly stochastic) map $\theta(\cdot) : \mathcal{X} \rightarrow \mathbb{R}^K$ learns a discriminative surrogate for the LLR $\Lambda(c, x)$ from samples, bypassing direct density estimation.

Then by the definitions of P and Q , we get:

$$D_{KL}(P\|Q) = \mathbb{E}_P \left[\log \frac{dP}{dQ} dP \right] \quad (8)$$

$$= \frac{1}{K} \sum_{c=1}^K \int_{\mathcal{X}} \log \frac{dX_c}{dX_{\bar{c}}}(x) dX_c(x) \quad (9)$$

$$= \frac{1}{K} \sum_{c=1}^K D_{KL}(X_c \| X_{\bar{c}}) := D_{inp}, \quad (10)$$

which defines a universal performance bound for the task at hand. Note that if the class conditionals have mismatched support, the divergence is infinite. See Appendix B.2 for a further discussion of the ramifications of this fact.

On the other hand, the classification layer of a neural network does not have access to the input variable X , but rather its own distilled representation $Z = \theta(X)$. Let now $Z_c = \mathbb{P}(Z|Y=c)$, $Z_{\bar{c}} = \mathbb{P}(Z|Y \neq c)$ be the class conditional distributions of the network representation Z . Then by the data processing inequality (DPI) for KL divergence (Polyanskiy & Wu, 2016), we have

$$D_{KL}(Z_c \| Z_{\bar{c}}) \leq D_{KL}(X_c \| X_{\bar{c}}), \forall c \quad (11)$$

since $Z_c = \theta(X_c)$ and similarly for $Z_{\bar{c}}$. Consequently the average divergence of the network conditionals is bounded by the input divergence:

$$D_{\theta} := \frac{1}{K} \sum_{c=1}^K D_{KL}(Z_c \| Z_{\bar{c}}) \leq D_{inp}. \quad (12)$$

Therefore, utilizing (3), we argue that the *NP-optimal* network solves the following equivalent objectives:

$$\max_{Z: Y - X - Z} \frac{1}{K} \sum_{c=1}^K D_{KL}(Z_c \| Z_{\bar{c}}) \quad (13)$$

$$= \frac{1}{K} \sum_{c=1}^K \lim_{n \rightarrow \infty} -\frac{1}{n} \log \beta_{c,n}^{*,Z}(\alpha), \quad (14)$$

where $\beta_{c,n}^{*,Z}(\alpha)$ is the *best* achievable false negative error rate in distinguishing class c , using representation Z , n samples and false positive error rate of at most α .

3.3. Evidence-Error Plane

We define a 2-D coordinate system (analogous to the Information Plane from (Shwartz-Ziv & Tishby, 2017)) where networks can be translated into points in terms of their type-II error rates versus retained KL divergence. Formally each network θ is mapped to a point on the positive quadrant of the real plane:

$$\Phi(\theta) = (P_{\theta}, D_{\theta}) \in \mathbb{R}_+^2, \quad (15)$$

where $P_{\theta} = -\log(\beta_{\theta})$ is the minus log of the empirically achieved type-II error rate of the network and D_{θ} is the average divergence between class conditioned representations produced by the network as defined in (12). This allows us to disentangle representation quality (characterized by divergence retained; the "evidence" axis) and how efficiently the network exploits its representations ("error" axis). Intuitively:

- Given two networks θ_1, θ_2 ; if $D_{\theta_1} \gg D_{\theta_2}$ but $P_{\theta_1} \approx P_{\theta_2}$, θ_2 is information inefficient, because excess KL is not converted to performance.
- For a single network θ ; if $P_{\theta} \ll D_{\theta}$ for high D_{θ} , the network is again information inefficient.

We can also interpret the $D_{\theta} = P_{\theta}$ envelope on the plane (which corresponds to the asymptotic Stein limit) as a performance boundary for the "best" networks, because they operate on the asymptotic limit of the uniformly most powerful hypothesis test. In other words, networks with $P_{\theta} \gg D_{\theta}$ significantly, *should not* exist. Moreover, due to DPI (11), the $D_{\theta} = D_{inp}$ line defines a bound on the y-axis. This allows us to characterize the achievable region for all networks as:

$$\mathcal{F} = \{(P_{\theta}, D_{\theta}) \in \mathbb{R}_+^2 : 0 \leq P_{\theta} \leq D_{\theta} \leq D_{inp}\}. \quad (16)$$

4. Experimental Results

We train different networks with comparable sizes/architectures and study their trajectories on the Evidence-Error plane. Each network consists of 4 hidden layers (64-32-16-8 neurons) and a Softmax classifier. All layers are fully connected and hidden layers have ReLU nonlinearities. The training is done via Cross Entropy loss on the logits, optimized via Adam (with learning rate $\gamma = 0.001$ and $\beta_1 = 0.9, \beta_2 = 0.999$) (Kingma & Ba, 2017). Each network is trained for 50 epochs. All experiments are implemented with the PyTorch framework (Paszke et al., 2019).

We estimate class-conditional KL divergences, both for the input distributions $D_{KL}(X_c \| X_{\bar{c}})$ and representations $D_{KL}(Z_c \| Z_{\bar{c}})$ using a k-nearest-neighbor (kNN)-based estimator, which approximates local density ratios from sample neighborhoods without any density modeling (Pérez-Cruz, 2008). Although it exhibits finite sample bias, the kNN estimator is asymptotically convergent (for any k) and in fact, known to be nearly minimax sample rate optimal in mean square error (Zhao & Lai, 2020). Coupled with the low computational demand, we deem it to be the ideal estimator for our application. All KL estimates are computed on full representation vectors (logit outputs of the classifier layer, before Softmax is applied) using identical settings

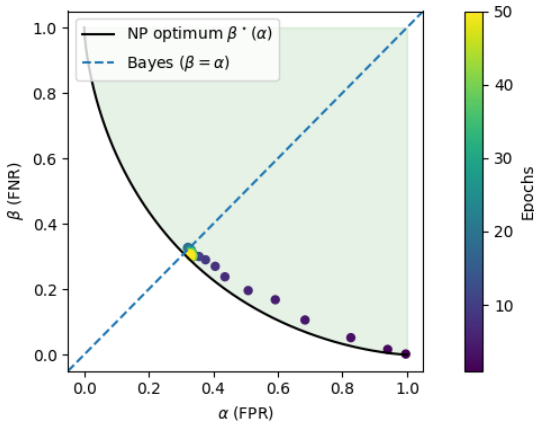


Figure 1: **4D Gaussian Dataset Error Rates:** Green region is all achievable error rates and the black curve defines the NP-optimal envelope. Each point is the empirical error rates of the network on the corresponding epoch. The network converges to the Bayes optimal classifier’s error rate, which is the intersection between the curve and the dotted line $\beta = \alpha$. See 4.1.

across layers and epochs. Appendix B.1 describes a heuristic for choosing k , among other bias reduction methods we employ.

4.1. Multivariate Gaussians

Before moving on to real (or realistic) datasets, we first study the case when the two classes are Gaussians as a sanity check. We generate two overlapping multivariate Gaussians with equal priors, unit covariance and a mean shifted only by one in the first coordinate. Formally: $X_0 \sim \mathcal{N}(\mu_0, I_d)$ and $X_1 \sim \mathcal{N}(\mu_1, I_d)$ with $\mu_0 = (0, 0, \dots, 0)$ and $\mu_1 = (1, 0, \dots, 0)$. Analytic KL divergence is symmetric and known in this case; $D_{KL}(X_0 \| X_1) = D_{KL}(X_1 \| X_0) = 0.5$ nats ≈ 0.721 bits.

Moreover, since they have unit covariance, the LLR test and associated error probabilities are:

$$(\mu_1 - \mu_0)^\top X \geq \gamma \quad (17)$$

$$\beta^*(\alpha) = \Phi(\Phi^{-1}(1 - \alpha) - \|\mu_1 - \mu_0\|_2) \quad (18)$$

where $\|\mu_1 - \mu_0\|_2 = 1$.

Figure 1 plots the empirical (α, β) error rates of a network on this dataset versus the NP optimal error envelope, $\beta^*(\alpha)$. The network exists nearly on the boundary and approaches the point intersecting the NP-optimal curve and the line corresponding to the Bayes error, $\beta = \alpha$ (since they have equal priors). This implies that the trained network is equivalent to the Bayes optimal classifier. Section 5 discusses this fact more in detail.

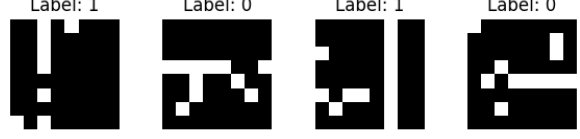


Figure 2: Sample points from the Binary Image Dataset

4.2. Networks on the Error-Evidence Plane

We move on to track the evolution of the same network architecture on the following datasets:

1. **Binary Image:** A custom toy dataset with binary classes and $d \times d$ images consisting of binary pixels, corrupted through a Binary Symmetric Channel (Polyanskiy & Wu, 2016) with bit flip probability p . See Appendix A for a detailed description of the data generation and KL divergence calculation. Sample images for $d = 8$ can be found in Figure 2.
2. **Yin-Yang:** A three class dataset (yin, yang and dot) generated by (x, y) coordinates on the unit disk. The coordinates $(1 - x, 1 - y)$ are also used as input features for symmetrizing the input ((Kriener et al., 2022)).
3. **MNIST:** The MNIST handwritten digits dataset, consisting of 28×28 grayscale images from 10 classes (LeCun, 1998).

Figure 3 presents the network trained on the Binary Image dataset with $d = 8$ and $p = 0.1$. This results in a relatively easy task that the network is able to solve in a handful of epochs. We observe that the network also converges, in the sense suggested by (13). Figure 4 shows the same network trained on MNIST, with a similar trajectory; although it is relatively information inefficient, as it is on average ~ 10.4 bits above the Stein limit.

4.3. $n > 1$ case: Majority Voting Classification

As argued before, Stein’s lemma only characterizes the $n \rightarrow \infty$ regime, where many i.i.d samples are tested simultaneously. However, typical neural networks operate at $n = 1$; because only a single input sample is processed for classification. To understand the effect of $n > 1$ samples being available at inference, we conduct the following experiment:

We train a network as usual, then generate $x = \{x_1, x_2, \dots, x_n\}$ i.i.d input samples all belonging to the same class c (equivalently, $x_i \sim X_c$ with high probability). At inference, we collect the network output on all samples $\Theta(x) = \{\theta(x_1), \theta(x_2), \dots, \theta(x_n)\}$ and perform a majority vot-

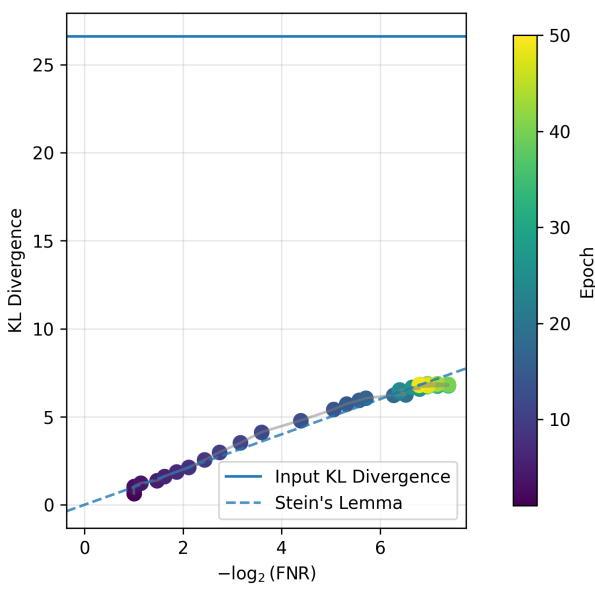


Figure 3: **DNN trained on Binary Image:** The network improves the KL divergence between its class conditioned representations as epochs increase and effectively exploits that divergence to reach the Stein error regime. This is the prototypical NP optimal neural network. The solid blue line denotes D_{inp} for this dataset and the dotted blue line is the predicted error rates from Stein’s Lemma.

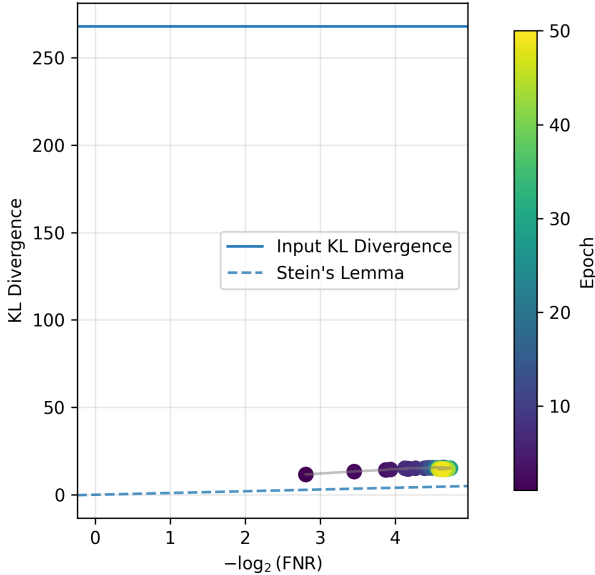


Figure 4: **DNN trained on MNIST:** The network trained on MNIST. A similar trajectory to Figure 3 is observed, although the network operates noticeably above the Stein limit.

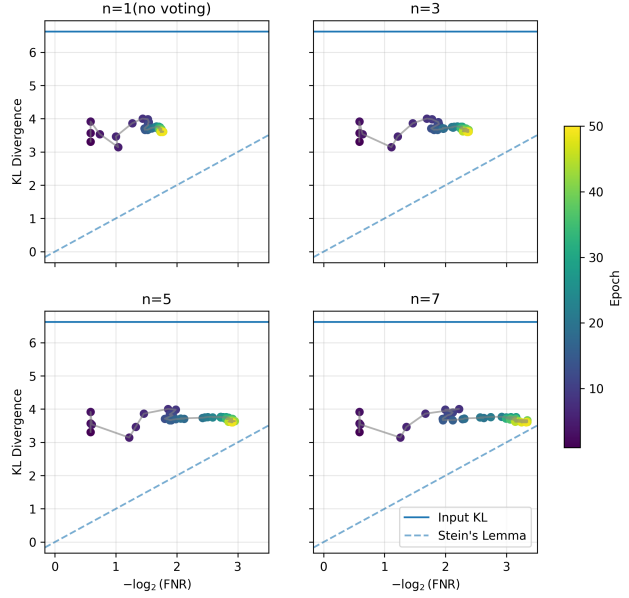


Figure 5: **Majority Voting on Information Inefficient Network:** A smaller network with only two hidden layers, trained on the Yin-Yang dataset and evaluated with majority voting classification. As the number of samples n used in the vote increase, the network performance also increases at the same classifier KL divergence level.

ing to determine class output:

$$\hat{y} = \operatorname{argmax}_{k \in \{1, \dots, K\}} \sum_{i=1}^n \mathbf{1}\{\theta(x_i) = k\}. \quad (19)$$

Then all x_i are classified as \hat{y} and error rates (α, β) are calculated as the result of that classification.

A priori, it is not the case that this would be equivalent to the LLR test on n samples. Moreover, it is not even true that error rates necessarily decline monotonically with n . See Appendix C.2 for a counterexample for this.

However, we observe that for networks that we have classified as “information inefficient” ($D_\theta \gg P_\theta$), majority voting indeed improves performance and allows the network to approach the Stein regime (See Figure 5).

Indeed, in early epochs when sufficient D_θ is not reached, majority voting does not provide a significant increase in P_θ ; whereas in later epochs the network moves significantly right on the P_θ axis. Therefore we observe the existence of a threshold type relation; where below a certain network divergence D_{th} , ensemble rules have no effect on P_θ .

4.4. Spiking Neural Networks

A separate class of neural networks we study are Spiking Neural Networks (SNNs), which implement discrete-time Leaky Integrate-and-Fire (LIF) neurons rather than standard perceptrons and are trained via surrogate gradient methods (Eshraghian et al., 2023). Each input sample x_i is encoded, via a fixed encoding scheme, into a binary spike train with $S_0[t] \in \{0, 1\}^d$ of length $\tau \in \mathbb{N}$, $t \in \{1, 2, \dots, \tau\}$. Neurons maintain an internal state referred to as the *membrane potential* $U_l[t]$, where l indexes the network layer. The membrane potential evolves according to

$$U_l[t] = \eta U_l[t-1] + W_{l-1} S_{l-1}[t] - V_{\text{th}} S_l[t-1], \quad (20)$$

$$S_l[t] = \Theta(U_l[t] - V_{\text{th}}) \quad (21)$$

where $\eta \in (0, 1)$ is the leak factor, W_{l-1} denotes the synaptic weight matrix from layer $l-1$ to layer l , V_{th} is a fixed firing threshold, and $\Theta(\cdot)$ is the Heaviside step function. After a neuron fires, its potential is reset by V_{th} .

This event-driven dynamics leads to sparse activations and, when deployed on neuromorphic hardware, enables substantial reductions in inference-time energy consumption (Kudithipudi et al., 2025). Due to the explicit notion of internal state given by the membrane potential, we analyze SNNs with the same architecture as their non-spiking counterparts and define class-conditional representations via $U_c = \mathbb{P}(U | Y = c)$ with $U_{\bar{c}}$ defined analogously.

We encode inputs via rate-coding using Poisson spike trains, where for each feature x_i , the spikes are sampled i.i.d. with $S_i[t] \sim \text{Bernoulli}(x_i)$ for $\tau = 5$ assuming normalized inputs. We take $\eta = 0.95$ constant and we train our model with the SNN Torch framework, using $S \approx \frac{1}{\pi} \arctan(\pi U)$ as the surrogate for backpropagation. (Eshraghian et al., 2023).

Figure 6 shows the Evidence-Error plane trajectory of the SNN on Binary Image. In contrast to DNN’s, we observe a two-phase trajectory (analogously to Information Bottleneck (Shwartz-Ziv & Tishby, 2017), although “reversed”); where the early epochs have constant error rates but dramatically increase classifier divergence (well above the equivalent DNN), and later epochs exploit that divergence by increasing P_θ .

However, for fixed weights W_l , note that the support of the membrane potential distribution is effectively a finite alphabet, as updates to the potential are done in discrete steps. Therefore the estimator may be unreliable. See Appendix C.1 for a detailed argument.

Finally, in Table 1, we report (D_θ, P_θ) pairs for different trained network architectures, as well as D_{inp} values for the respective datasets.

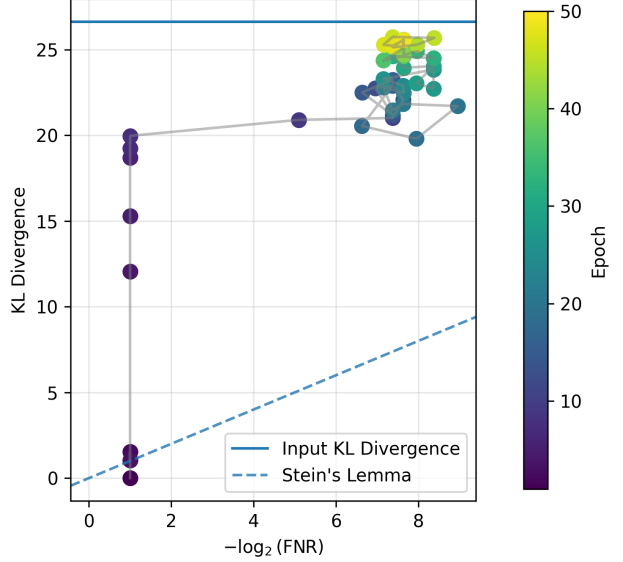


Figure 6: **SNN trained on Binary Image:** A dramatic increase in classifier divergence in early epochs followed by a “fitting” phase of performance increase in later epochs. See 4.4.

5. Conclusion and Future Work

In this work, we argued theoretically that neural classifier performance can be characterized in terms of binary hypothesis testing and achievable type-II error (β) based on representation quality. By embedding model trajectories during training into an evidence–error coordinate plane, we disentangled the information available in learned representations from how efficiently it is exploited by the decision rule, and showed that effective training moves networks inside an information-theoretic achievable region, defined by the available divergence between class conditionals and corresponding reachable error rates.

The values we have defined like classifier divergence D_θ (12), can be used for justifiable model selection, explaining architecture strengths/limitations and possibly be formulated as quantities to be regularized during training. Moreover, the effects of majority voting on classifier performance can be quantified through the error-evidence plots and a relation between performance improvement from majority voting (or other ensemble classification rules) and D_θ can be derived.

We note however, the main shortcoming of our analysis: in reality, neural network loss functions typically minimize type-I and type-II errors simultaneously. This (Bayesian) setup can be expressed as:

$$P_e^* = \min_{\text{Test}} \pi_P \alpha_n + \pi_Q \beta_n \quad (22)$$

where π_P, π_Q are the priors of the hypotheses P and Q . We

Table 1: (D_θ, P_θ) values for trained classifiers with different architectures. Overall most information efficient network is highlighted. The input divergence D_{inp} for each dataset is also given as reference.

Model Type	Binary Image (26.6)	Yin-Yang (6.3)	MNIST (258.8)
Fully Connected (FC)	(7.5, 7.3)	(4.0, 2.6)	(14.8, 4.6)
FC + BatchNorm	(7.0, 6.0)	(5.8, 4.2)	(20.7, 5.0)
FC + Dropout	(7.9, 7.2)	(4.9, 2.2)	(29.2, 4.2)
FC + Residual Blocks	(7.8, 7.4)	(4.6, 2.4)	(15.9, 4.7)
Conv1D	(6.5, 6.8)	(3.9, 2.75)	(6.3, 1.4)
SNN	(25.1, 7.3)	(5.0, 1.2)	(238.0, 4.4)
Linear	(0.9, 1.0)	(3.7, 1.0)	(8.9, 3.7)

have briefly observed this in the Gaussian case (see again Figure 1) where the network converges exactly to P_e^* .

For the asymptotic case of Bayesian error, analogous to Stein’s lemma, the Chernoff Information between P and Q defines the optimal error exponent (assuming a common measure μ for P and Q) (Chernoff, 1952):

$$\lim_{n \rightarrow \infty} -\frac{1}{n} \log(P_e^*) = -\log \min_{0 \leq \lambda \leq 1} \left\{ \left(\int p(\mu)^\lambda q(\mu)^{1-\lambda} d\mu \right) \right\} \quad (23)$$

$$:= C(P, Q) \quad (24)$$

and can equivalently be stated as the following KL divergence:

$$C(P, Q) = D_{KL}(P_{\lambda^*} \| P) = D_{KL}(P_{\lambda^*} \| Q) \quad (25)$$

where

$$P_\lambda(z) = \frac{P^\lambda(z)Q^{1-\lambda}(z)}{\int P^\lambda(\mu)Q^{1-\lambda}(\mu)d\mu} \quad (26)$$

and λ^* is the value of λ maximizing the first expression. Note that the priors vanish in the asymptotics and $C(P, Q) = C(Q, P)$, unlike KL divergence.

Analytic forms of $C(P, Q)$ beyond a handful of distributions, e.g (Nielsen, 2011) are not known and estimating it is difficult due to the effective optimization over distributions through λ . To the best of our knowledge, no reliable kNN estimator even exists.

Therefore, the Neyman-Pearson analysis presented here should be interpreted as a deliberate simplification, in which the network’s false positive rate is effectively discarded. A natural extension would be to examine whether networks operate near the Chernoff optimal regime in the evidence–error plane.

Impact Statement

We presented a deeper theoretical understanding of a wide-class of deep neural network models. The presented analysis

provides a better understanding of neural network training dynamics and connects it with the well studied Neyman-Pearson test. The described process also helps to study neural networks from the aspects of error rates that make their performance more quantifiable from a statistical risk perspective, an essential requirement for deployment in safety-critical applications.

References

Anders, U. and Korn, O. Model selection in neural networks. *Neural networks*, 12(2):309–323, 1999.

Chernoff, H. A measure of asymptotic efficiency for tests of a hypothesis based on the sum of observations. *The Annals of Mathematical Statistics*, pp. 493–507, 1952.

Chernoff, H. Large-sample theory: Parametric case. *The Annals of Mathematical Statistics*, 27(1):1–22, 1956.

Eshraghian, J. K., Ward, M., Neftci, E. O., Wang, X., Lenz, G., Dwivedi, G., Bennamoun, M., Jeong, D. S., and Lu, W. D. Training spiking neural networks using lessons from deep learning. *Proceedings of the IEEE*, 111(9):1016–1054, 2023.

Kingma, D. P. and Ba, J. Adam: A method for stochastic optimization, 2017. URL <https://arxiv.org/abs/1412.6980>.

Kolchinsky, A., Tracey, B. D., and Van Kuyk, S. Caveats for information bottleneck in deterministic scenarios. *arXiv preprint arXiv:1808.07593*, 2018.

Kriener, L., Göltz, J., and Petrovici, M. A. The yin-yang dataset. In *Proceedings of the 2022 Annual Neuro-Inspired Computational Elements Conference*, pp. 107–111, 2022.

Kudithipudi, D., Schuman, C., Vineyard, C. M., Pandit, T., Merkel, C., Kubendran, R., Aimone, J. B., Orchard, G., Mayr, C., Benosman, R., et al. Neuromorphic computing at scale. *Nature*, 637(8047):801–812, 2025.

Kullback, S. and Leibler, R. A. On information and sufficiency. *The annals of mathematical statistics*, 22(1):79–86, 1951.

LeCun, Y. The mnist database of handwritten digits. <http://yann.lecun.com/exdb/mnist/>, 1998.

Mandel, F. and Barnett, I. Permutation-based hypothesis testing for neural networks. In *Proceedings of the AAAI Conference on Artificial Intelligence*, volume 38, pp. 14306–14314, 2024.

Montavon, G., Binder, A., Lapuschkin, S., Samek, W., and Müller, K.-R. Layer-wise relevance propagation: an

overview. *Explainable AI: interpreting, explaining and visualizing deep learning*, pp. 193–209, 2019.

Neyman, J. and Pearson, E. S. IX. on the problem of the most efficient tests of statistical hypotheses. *Philosophical Transactions of the Royal Society of London. Series A, Containing Papers of a Mathematical or Physical Character*, 231(694-706):289–337, 1933.

Nielsen, F. Chernoff information of exponential families. *arXiv preprint arXiv:1102.2684*, 2011.

Paszke, A., Gross, S., Massa, F., Lerer, A., Bradbury, J., Chanan, G., Killeen, T., Lin, Z., Gimelshein, N., Antiga, L., et al. Pytorch: An imperative style, high-performance deep learning library. *Advances in neural information processing systems*, 32, 2019.

Pérez-Cruz, F. Kullback-leibler divergence estimation of continuous distributions. In *2008 IEEE international symposium on information theory*, pp. 1666–1670. IEEE, 2008.

Polyanskiy, Y. and Wu, Y. Lecture notes on information theory. MIT OpenCourseWare, 2016. URL <https://ocw.mit.edu/courses/6-441-information-theory-spring-2016/>. Course 6.441, Spring 2016.

Rawal, K., Fu, Z., Delaney, E., and Russell, C. Evaluating model explanations without ground truth. In *Proceedings of the 2025 ACM Conference on Fairness, Accountability, and Transparency*, pp. 3400–3411, 2025.

Ribeiro, M. T., Singh, S., and Guestrin, C. "why should i trust you?" explaining the predictions of any classifier. In *Proceedings of the 22nd ACM SIGKDD international conference on knowledge discovery and data mining*, pp. 1135–1144, 2016.

Saxe, A. M., Bansal, Y., Dapello, J., Advani, M., Kolchinsky, A., Tracey, B. D., and Cox, D. D. On the information bottleneck theory of deep learning. *Journal of Statistical Mechanics: Theory and Experiment*, 2019(12):124020, 2019.

Shwartz-Ziv, R. and Tishby, N. Opening the black box of deep neural networks via information. *arXiv preprint arXiv:1703.00810*, 2017.

Tax, T. M., Mediano, P. A., and Shanahan, M. The partial information decomposition of generative neural network models. *Entropy*, 19(9):474, 2017.

Wang, Q., Kulkarni, S. R., and Verdú, S. Divergence estimation for multidimensional densities via k -nearest-neighbor distances. *IEEE Transactions on Information Theory*, 55(5):2392–2405, 2009.

Wang, Z. and Scott, D. W. Nonparametric density estimation for high-dimensional data—algorithms and applications. *Wiley Interdisciplinary Reviews: Computational Statistics*, 11(4):e1461, 2019.

Westphal, C., Hailes, S., and Musolesi, M. A generalized information bottleneck theory of deep learning. *arXiv preprint arXiv:2509.26327*, 2025.

Zhang, Y., Tiño, P., Leonardis, A., and Tang, K. A survey on neural network interpretability. *IEEE transactions on emerging topics in computational intelligence*, 5(5):726–742, 2021.

Zhao, P. and Lai, L. Minimax optimal estimation of kl divergence for continuous distributions. *IEEE Transactions on Information Theory*, 66(12):7787–7811, 2020.

Zhu, Z., Ding, T., Zhou, J., Li, X., You, C., Sulam, J., and Qu, Q. A geometric analysis of neural collapse with unconstrained features. *Advances in Neural Information Processing Systems*, 34:29820–29834, 2021.

A. Binary Image Toy Dataset

We create a two-class, binary dataset with controllable parameters and tractable KL. Let $d \in \mathbb{N}$ be a dimension parameter and $p \in (0, 1)$ a noise probability. Then our sample space is defined as:

$$\mathcal{X} = \{0, 1\}^{d \times d}. \quad (27)$$

We define two class-conditional distributions corresponding to the hypotheses H_R : row-white images vs. H_C : column-white images with equal priors. Under H_R , a row index is sampled uniformly in the dimension, $r \sim \mathcal{U}\{1, d\}$ and a template is generated as:

$$T_{ij}^{(r)} = \mathbf{1}\{i = r\} \quad (28)$$

that is, the r -th row is set to one and all remaining pixels are zero. The observed image X is obtained by passing $T^{(R)}$ through an independent Binary Symmetric Channel with flip probability $p \in (0, 1)$:

$$X_{ij} = \begin{cases} T_{ij}^{(r)} & \text{with probability } 1 - p, \\ 1 - T_{ij}^{(r)} & \text{with probability } p, \end{cases} \quad (29)$$

A similar process is followed for columns under H_C ($U_{ij}^{(c)} = \mathbf{1}\{j = c\}$ for $c \sim \mathcal{U}\{1, d\}$).

Note that the distribution of this dataset is supported on a finite alphabet and therefore the kNN KL estimator may not work well, especially for small d due to distance ties and degenerate neighborhood volumes (Wang et al., 2009). However the same argument can be made for standard image datasets like MNIST and CIFAR-10 where pixel values are integer-valued (therefore distributed on a finite alphabet) but are commonly treated as embedded in a continuous Euclidean space. Following this convention, we find empirically that for moderate d , the induced geometry is sufficient for stable estimation. We therefore fix $d = 8$ (and $p = 0.1$) as the canonical setting.

We can derive the true KL divergence of this dataset as follows: first let P_R and P_C denote the row-white and column-white image conditionals on $\mathcal{X} = \{0, 1\}^{d \times d}$. Then we have

$$D_{KL}(P_R \| P_C) = \mathbb{E}_{X \sim P_R} \left[\log \frac{P_R(X)}{P_C(X)} \right] \quad (30)$$

We can condition the marginals on the templates t^r and u^c representing the r -th row and c -th column white images (a.k.a uncorrupted)

$$D_{KL}(P_R \| P_C) = \mathbb{E}_{X \sim P_R} \left[\log \frac{\sum_{r=1}^d P(X|t^r)}{\sum_{c=1}^d P(X|u^c)} \right] \quad (31)$$

since the uniform probability of picking r or c cancels out. Now for any template $s \in \{0, 1\}^{d \times d}$, we can express the conditional likelihood under BSC noise for any image as:

$$P(x | s) = \prod_{i=1}^d \prod_{j=1}^d \begin{cases} 1 - p & \text{if } x_{ij} = s_{ij}, \\ p & \text{if } x_{ij} \neq s_{ij}, \end{cases} \quad (32)$$

Denote the Hamming distance (pixels where they differ) between x and s as $d_H(x, s)$. Then we get the simplification

$$P(x | s) = (1 - p)^{d^2 - d_H(x, s)} p^{d_H(x, s)} = (1 - p)^{d^2} \left(\frac{p}{1 - p} \right)^{d_H(x, s)} = (1 - p)^{d^2} \lambda^{d_H(x, s)} \quad (33)$$

where $\lambda = \frac{p}{1-p}$. Substituting this back into KL:

$$D_{KL}(P_R \| P_C) = \mathbb{E}_{X \sim P_R} \left[\log \frac{\sum_{r=1}^d \lambda^{d_H(x, t^r)}}{\sum_{c=1}^d \lambda^{d_H(x, u^c)}} \right] \quad (34)$$

since the constants $(1 - p)^d$ cancel. Now we need to derive expressions for the distance terms, starting with the row cases:

$$d_H(x, t^r) = \sum_{i=1}^d \sum_{j=1}^d \mathbf{1}\{x_{ij} \neq t_{ij}^r\} = \sum_{j=1}^d \mathbf{1}\{x_{rj} \neq t_{rj}^{(r)}\} + \sum_{\substack{i=1 \\ i \neq r}}^d \sum_{j=1}^d \mathbf{1}\{x_{ij} \neq t_{ij}^{(r)}\} \quad (35)$$

$$= d - a_r(x) + T(x) - a_r(x) = d - 2a_r(x) + T(x) \quad (36)$$

where $T(x)$ is the sum over x (meaning the number of ones in x) and $a_r(x)$ is the sum of the r -th row of x ; the number of ones in row r of x . We can do a similar calculation to get:

$$d_H(x, u^{(c)}) = d + T(x) - 2b_c(x) \quad (37)$$

for the column templates with $b_c(x)$ as the number of ones in column c of x . Plugging these distances back into the KL term, we observe that again $\lambda^{d+T(x)}$ cancels in each term:

$$D_{KL}(P_R \| P_C) = \mathbb{E}_{X \sim P_R} \left[\log \frac{\sum_{r=1}^d \lambda^{-2a_r(x)}}{\sum_{c=1}^d \lambda^{-2b_c(x)}} \right] := \mathbb{E}_{X \sim P_R} [\phi(X)] \quad (38)$$

by renaming the LLR as $\phi(X)$. Since P_R is generated by uniformly sampling row values $r \sim U\{1, d\}$ (and the same for P_C) we can express the expectation as follows:

$$D_{KL}(P_R \| P_C) = \frac{1}{d} \sum_{r=1}^d \mathbb{E}_{X \sim P(\cdot | t^r)} [\phi(X)] \quad (39)$$

Under a fixed template t^r , the pixels are distributed as independent Bernoulli variables, $X \sim P(\cdot | t^r)$:

$$X_{ij} \sim \begin{cases} \text{Bern}(1 - p) & \text{if } i = r, \\ \text{Bern}(p) & \text{otherwise} \end{cases} \quad (40)$$

Therefore we can express the distributions $A_i = a_i(X)$ as binomials since they are the sums of pixel values distributed as i.i.d. Bernoulli variables. This gives us:

$$A_i \sim \text{Bin}(d, p) \quad \forall i \neq r \text{ and } A_r \sim \text{Bin}(d, 1 - p) \quad (41)$$

For the column variables, $B_j = b_j(X) = \sum_{i=1}^d X_{ij}$ we have to consider the pixel on the active row $i = r$ as a separate case since $X_{rj} \sim \text{Bern}(1 - p)$ while $X_{ij} \sim \text{Bern}(p)$ for $i \neq r$. Then we get:

$$B_j = \text{Bern}(1 - p) + \text{Bin}(d - 1, p) \quad (42)$$

Plugging these distributions and taking the expectation of $\phi(X)$ (omitting subscript $X \sim P(\cdot | t^r)$):

$$\mathbb{E}[\phi(X)] = \mathbb{E}[\log \left(\sum_{i=1}^d \lambda^{-2A_i} \right)] - \mathbb{E}[\log \left(\sum_{j=1}^d \lambda^{-2B_j} \right)] \quad (43)$$

$$:= E_{row}(d, p) - E_{col}(d, p) \quad (44)$$

where E_{row} and E_{col} have closed form expressions in (d, p) (omitted here for brevity) since A_i and B_j have distributions depending only in d, p and are independent of the row choice r . Therefore the sum over rows cancels the $\frac{1}{d}$ factor outside and we are left simply with:

$$D_{KL}(P_R \| P_C) = E_{row}(d, p) - E_{col}(d, p) \quad (45)$$

Figure 7 tracks the change of $D_{KL}(P_R \| P_C)$ with d and p and compares it to the kNN estimator.

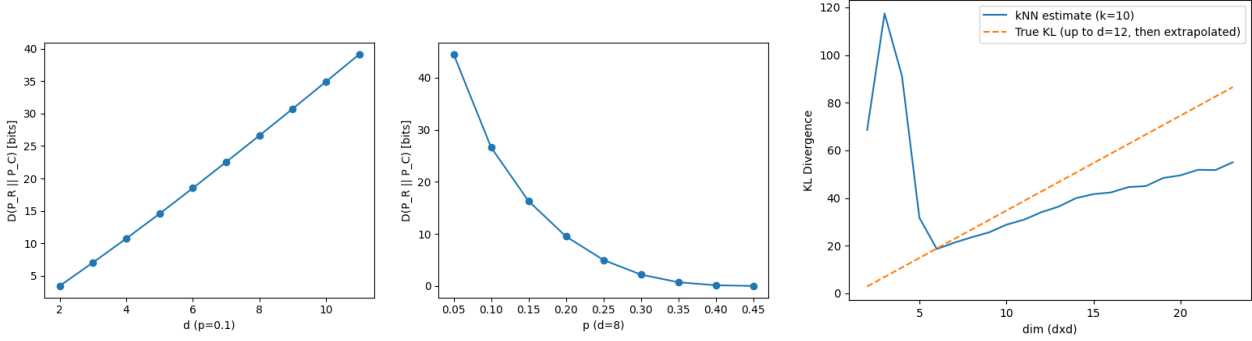


Figure 7: **KL Divergence of the Binary Image Dataset and its kNN Estimate:** We observe that for dimensions in the range 6-15, estimation is reliable but as d grows, the downward bias becomes non-negligible. As discussed, for small d , the estimator likely explodes due to the small alphabet size of the underlying event space.

B. kNN Estimation of KL Divergence

B.1. Finite Sample Bias

The proposed kNN estimators in (Pérez-Cruz, 2008) and (Wang et al., 2009), which we extensively utilize in our experiments, are known to be consistent for any value of k , asymptotically. However with finite samples, they are biased; this bias typically scales with dimension. (Wang et al., 2009) suggests using adaptive k values pointwise for good log-density ratio estimation, which is proven to achieve optimal bias/variance trade-offs but is also computationally expensive.

To overcome the finite sample bias with negligible compute overhead, we use the following simple heuristic for selecting k in a data dependent way. (Note that we don't claim any guarantees or bias bounds as this depends on the geometry of the underlying distribution):

Algorithm 1 Null-Consistency Selection of k for kNN Divergence Estimation

```

Input: Dataset  $\mathcal{X} = \{x_i\}_{i=1}^N$ , candidate set  $\mathcal{K}$ , number of splits  $S$ 
Initialize  $k^* = 1$ 
for  $k \in \mathcal{K}$  do
    for  $s = 1$  to  $S$  do
        Randomly split  $\mathcal{X}$  into two disjoint subsets  $\mathcal{X}_1^{(s)}$  and  $\mathcal{X}_2^{(s)}$ 
        Compute  $\hat{D}_k^{(s)} \leftarrow \hat{D}_k\left(\mathcal{X}_1^{(s)} \parallel \mathcal{X}_2^{(s)}\right)$ 
    end for
    Compute empirical average null bias:  $b_k \leftarrow \frac{1}{S} \sum_{s=1}^S \hat{D}_k^{(s)}$ 
end for
 $k^* \leftarrow \arg \min_{k \in \mathcal{K}} |b_k|$ 
output  $k^*$ 

```

Since the true divergence of any distribution X with itself $D_{KL}(X\|X) = 0$, this procedure outputs the k that is most stable in low divergence regimes.

Furthermore (Zhao & Lai, 2020) notes that when the data lives on a lower-dimensional manifold than its original dimension, the kNN estimator has upward bias as the neighborhoods grow disproportionately. This bias again scales exponentially with dimension. Since neural network logits of a classifier with K outputs is known to collapse to a $K - 1$ dimensional manifold (so-called neural collapse (Zhu et al., 2021)), we apply a change of coordinate before network outputs are fed into the KL estimator. Formally:

Let $Z = (Z_1, \dots, Z_K)^\top \in \mathbb{R}^K$ be the logit vector. Then we have $\text{Softmax}(Z) = \text{Softmax}(Z + c\mathbf{1})$ for any constant

$c \in \mathbb{R}$. Without loss of generality, (as it can be defined for any reference class) define the following projection $\Pi \in \mathbb{R}^{K \times K-1}$:

$$u = \Pi Z = (Z_1 - Z_K, \dots, Z_{K-1} - Z_K)^\top \in \mathbb{R}^{K-1}. \quad (46)$$

Then $\Pi(Z + K\mathbf{1}) = \Pi Z$ and

$$\text{Softmax}(Z)_i = \frac{e^{u_i}}{1 + \sum_{j=1}^{K-1} e^{u_j}} \quad (47)$$

with $u_K := 0$ for completeness. So u is a minimal sufficient, shift-invariant representation of the logits and we can estimate KL divergence on samples of u instead of Z .

B.2. Singularities in KL-Divergence

Recall that the KL divergence between P and Q can be infinite, in the case when P is not *absolutely continuous* with respect to Q , i.e.,

$$\exists A \subset \mathcal{X} \text{ measurable such that } P(A) > 0 \text{ and } Q(A) = 0. \quad (48)$$

Far from being an edge case, this can easily happen when we define P and Q as the class conditioned distributions; when $y = f(x)$ for a pair (x, y) and deterministic f , we immediately have $P(x, y) > 0$ while $Q(x, y) = 0$; in fact the distributions X_c and $X_{c'}$ may have completely disjoint support for class pairs c, c' .

To ensure absolute continuity between class conditionals, we inject a small amount of white noise to each input sample before it is fed into the divergence estimator. Note that unless the corrupted samples are fed into the network, DPI does not hold. Formally let $\tilde{X}_c^\sigma = X_c + \mathcal{N}(0, \sigma^2)$ and $\tilde{Z}_c = \theta(\tilde{X}_c^\sigma)$ with θ , the network. Then, we *only* have the chain:

$$D_{KL}(X_c \| X_{\bar{c}}) > D_{KL}(\tilde{X}_c^\sigma \| \tilde{X}_{\bar{c}}^\sigma) \geq D_{KL}(\tilde{Z}_c \| \tilde{Z}_{\bar{c}}) \quad (49)$$

regardless of whether $X_c \ll X_{\bar{c}}$ or $X_c \not\ll X_{\bar{c}}$. In the small noise limit we recover

$$\lim_{\sigma \rightarrow 0} D_{KL}(\tilde{X}_c^\sigma \| \tilde{X}_{\bar{c}}^\sigma) = D_{KL}(X_c \| X_{\bar{c}}) \quad (50)$$

To observe the effect of this noise on the estimators (see Figure 8), we sweep across a logarithmic range of additive noise values and track the estimator output $D_\sigma(X) = \frac{1}{K} \sum_{c \in Y} \hat{D}(\tilde{X}_c^\sigma \| \tilde{X}_{\bar{c}}^\sigma)$. We observe that for noise values with roughly $\sigma < 10^{-3}$, the added noise has negligible effect on the estimated KL, while ensuring theoretical consistency. Therefore for all our experiments we inject noise with $\sigma = 10^{-6}$.

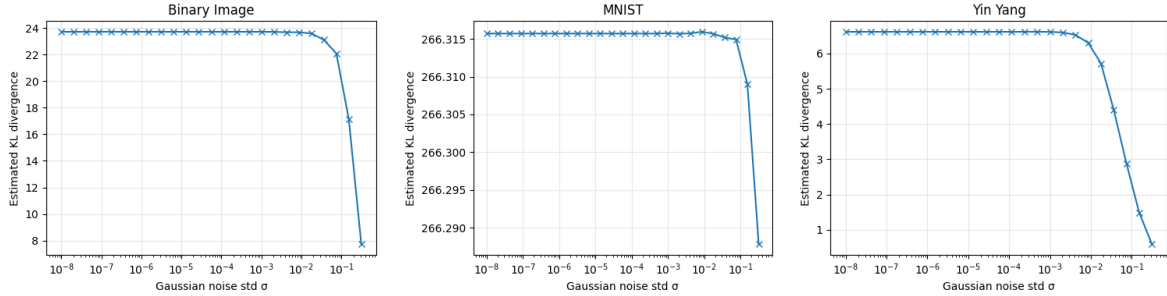


Figure 8: **Effect of additive noise on KL Div estimates:** Note that for noise values below 10^{-3} , the estimates are stable.

C. Experimental Details

C.1. SNN Membrane Potential Distribution Support Size

Recall the Leaky-Integrate Fire neuron dynamics:

$$U_l[t] = \eta U_l[t-1] + W_{l-1} S_{l-1}[t] - V_{\text{th}} S_l[t-1], \quad S_l[t] = \Theta(U_l[t] - V_{\text{th}}) \quad (51)$$

and note that $t \in \{1, 2, \dots, \tau\}$ for $\tau \in \mathbb{N}$ constant (in our experiments $\tau = 5$). Without loss of generality, assume a single neuron for each layer to simplify computation. Since each spike event is binary, the number of possible values of U_l given a fixed weight W_{l-1} is constant. Observe that each update adds one of 4 values:

$$\Delta U_l[t] \in \{0, W_{l-1}, -V_{\text{th}}, W_{l-1} - V_{\text{th}}\}. \quad (52)$$

and since $U_l[0] = 0$, the unrolled $U_l[t]$ is:

$$U_l[t] = \sum_{k=1}^t \eta^{t-k} (W_{l-1} S_{l-1}[k] - V_{\text{th}} S_l[k-1]) \quad (53)$$

Therefore

$$|\text{supp}(U_l[t])| \leq 4^t \rightarrow |\text{supp}(\{U_l[t]\}_{t=1}^\tau)| \leq \sum_{t=1}^\tau 4^t = \frac{4^{\tau+1} - 4}{3} \quad (54)$$

C.2. Counter Example for Majority Voting

Consider a binary classifier θ and 3 samples: $(x_1, x_2, x_3) \sim P^{\otimes 3}$ from the same class with the following probability of error

$$p := \mathbb{P}[\theta(x) \neq Y|Y] \quad (55)$$

Let now θ_{maj} be the majority classifier using θ on 3 samples. Then the error probability of θ_{maj} is:

$$p_{maj} := \mathbb{P}[\theta_{maj}(x_1, x_2, x_3) \neq Y|Y] = \mathbb{P}[\text{at least 2 samples are classified wrong}] \quad (56)$$

$$= \binom{3}{2} p^2 (1-p) + p^3 = 3p^2 - 2p^3 \quad (57)$$

Then for any $p \in (\frac{1}{2}, 1)$, we have that $p_{maj} > p$; though arguably this is not very realistic as $p \in (\frac{1}{2}, 1)$ corresponds to worse than random classification.